Journal of Inorganic and General Chemistry
ZAAC
Zeitschrift für anorganische und allgemeine Chemie
www.zaac.wiley-vch.de
RESEARCH ARTICLE

DOI: 10.1002/zaac.202500171

Synthesis and Characterization of the Ternary Carbodiimide $Na_2Hf(NCN)_3$

Hicham Bourakhouadar, Juan Medina-Jurado, Linda S. Reitz, Lothar Schrey, Alex J. Corkett,* and Richard Dronskowski*

In memoriam Prof. Rüdiger Kniep

$Na_2Hf(NCN)_3$ was prepared via a solid-state metathesis reaction between Na_2NCN and $HfCl_4$. Its crystal structure was determined from powder X-ray diffraction data and found to crystallize in a low-symmetry variant of the [NiAs] type with space group $R\bar{3}c$. It may, therefore, be described as a hexagonally close-packed array of NCN^{2-} dianions orientated along the *c*-axis, with metal cations occupying the octahedral voids in an ordered fashion. Rietveld analysis reveals a site mixing between sodium at the 12*c* site and hafnium at the 6*b* site in the order of 12(1)%. Moreover, both IR measurements and density functional theory calculations are consistent with a bent carbodiimide, presumably in order to accommodate metals with considerable differences in size within the same layer. The experimental optical band gap was measured to 4.1 eV coherent with the white colored sample.

1. Introduction

The rather mild solid-state metathesis (SSM) reaction has enabled the synthesis of a large number of endothermic metastable phases that incorporate the dinitridocarbonate NCN^{2-} unit, in either its symmetrical $^{-}N{=}C{=}N^{-}$ carbodiimide or asymmetrical $N{\equiv}C{-}N^{2-}$ cyanamide form. These types of reactions have demonstrated great versatility in the preparation of compounds incorporating alkali metals, transition metals, and also rare-earth metals into this class of structures.[1] The general concept of the SSM is to use a tailored mixture of precursors to promote an exothermic exchange of the constituent ions to form the desired product and a co-produced salt, which provides the driving force for the reaction.

This means that a precursor already containing the NCN^{2-} group is required. The most common examples for such precursors are Li_2NCN, Na_2NCN, or ZnNCN.[2–4]

A typical SSM reaction using Na_2NCN as a precursor, reacting with halides (where *M*X is generally either a chloride or a fluoride), can be described as in the following examples for the preparation of binary *M*NCN compounds and the ternary $NaM(NCN)_2$ compound.

$$Na_2NCN + MX_2 \rightarrow M(NCN) + 2NaX \quad (1)$$

$$2Na_2NCN + MX_3 \rightarrow NaM(NCN)_2 + 3NaX \quad (2)$$

A synthetic approach based on this scheme, however, has the inherent limitation of requiring suitable reagents, i.e., metal halides, that are stable at the temperatures required for such reactions (400–700 °C). Moreover, it has been demonstrated that the presence of NCN^{2-} at moderate temperatures can induce the reduction of the participating metal cations, resulting in carbodiimide products with metals in lower oxidation states than expected.[5] In addition, the use of Na_2NCN or Li_2NCN, which are unstable in air, dictates the use of an inert reaction atmosphere, since small amounts of moisture or oxygen lead to the formation of the more stable corresponding oxides. The synthetic challenge is, therefore, to control these factors.

For reasons of packing efficiency, metal carbodiimides and cyanamides frequently adopt layered structures with alternating sequences of metal cations and NCN^{2-}. In the absence of metals with stereochemically active lone pairs two packing motifs typically dominate in *M*(NCN) binary metal carbodiimides: [NiAs]-derived structures with a hexagonal close-packed arrangement of NCN^{2-} for *M* = Fe, Co, and Ni or [NaCl]-derived structures with cubic close-packed $[NCN]^{2-}$ for *M* = Mg, Ca, Sr, Cd, and Mn.[6–11] In contrast to binary carbodiimides, ternary NCN-containing compounds typically adopt NiAs rather than NaCl derived structures, whereby different arrangements of the metal cations are observed depending on the stoichiometry.[12] In the composition $AM(NCN)_2$ with *A* = Li or Na and *M* = Al, In, Y, Yb, and Sc, a hettotypic modification of the CoNCN structure is adopted due to the 1:1 ordering of cations on octahedral sites in channels perpendicular to the stacking direction, hence leading to orthorhombic structures with *Pbcn* symmetry.[13–16] A similar structure was recently reported for

H. Bourakhouadar, J. Medina-Jurado, L. S. Reitz, L. Schrey, R. Dronskowski
Chair of Solid-State and Quantum Chemistry, Institute of Inorganic Chemistry, RWTH Aachen University, 52056 Aachen, Germany
E-mail: drons@HAL9000.ac.rwth-aachen.de
A. J. Corkett
Jülich Center for Neutron Science-2 (JCNS), Forschungszentrum Jülich GmbH, 52425 Jülich, Germany
E-mail: alexander.corkett@ac.rwth-aachen.de

$MnCr_2(NCN)_4$, where Mn^{2+} and Cr^{3+} ions form single or double zigzag chains, respectively, also perpendicular to the stacking plane of the NCN^{2-}.[17] A different situation is observed, however, when larger cations are incorporated, as in $LiLa(NCN)_2$ where, instead of observing a layered structure, there is a monoclinic ($P2_1/m$) arrangement where the anions NCN^{2-} are arranged along two (rather than one) directions.[18] As already alluded to, the introduction of cations in higher oxidation states to ternary metal carbodiimides is a challenge due to the reducing character of the NCN^{2-} anion at moment of the synthesis.[5] Nonetheless, it is still possible to obtain compounds containing tetravalent cations where this oxidation state is the most stable option (i.e., for d^0 or d^{10} cations such as Hf^{4+}, Zr^{4+} and Sn^{4+}). This is the case in compounds with the formula $Li_2T(NCN)_3$ where an orthorhombic (*Pnna*) hettotype is encountered for T = Sn and a rhombohedral ($R\bar{3}c$) modification for T = Zr or Hf.[19] In this article, we present the synthesis and characterization of a further example containing a tetravalent cation, namely $Na_2Hf(NCN)_3$, a ternary carbodiimide that was prepared from $HfCl_4$ and Na_2NCN via an SSM.

2. Results and Discussion

$Na_2Hf(NCN)_3$ was prepared via a SSM reaction between Na_2NCN and $HfCl_4$, driven by the formation of the metathesis salt NaCl. After washing the product with water, powder X-ray diffraction (PXRD) data were collected, and the resulting reflections were indexed to a hexagonal unit cell with parameters $a = b = 6.23(4)$ Å, $c = 28.92(9)$ Å, slightly larger than those of the reported lithium-containing analog ($a = 5.776$ Å, $c = 28.803$ Å).[19] An initial structural model for $Na_2Hf(NCN)_3$ was therefore generated from that of $Li_2Hf(NCN)_3$ by replacing lithium with sodium at the 12*c* site. The model was subsequently refined using the GSAS suite, yielding poor agreement with the observed data ($R_{wp} = 9.23\%$), suggesting the presence of structural disorder. Indeed, further refinements allowing partial disorder between the Na and Hf positions, while constraining both sites to full occupancy, led to improved agreement with the observed data and indicated a cation site disorder of 12(1)%. The thermal displacement parameters (U_{iso}) of cations at the same site were constrained to be equal, as were the U_{iso}'s for all nonmetal atoms (C and N). The results are presented in **Figure 1** while the crystallographic data along with derived bond lengths and angles are summarized in **Table 1** and **2**, respectively.

The crystal structure of $Na_2Hf(NCN)_3$ exhibits a distorted hexagonal close-packed array of NCN^{2-} with metal cations occupying all of the octahedral holes. The average Na—N distance of 2.505(7) Å is very similar to that in $NaSc(NCN)_2$ (2.523 Å),[16] and the average Hf—N distance of 2.187(5) Å is similar to that in $Li_2MnHf_2(NCN)_6$ (2.16 Å),[20] consistent with the presence of a tetravalent hafnium.

A single crystallographically independent NCN unit is present in $Na_2Hf(NCN)_3$, which appears to be slightly distorted, indicated by the N—C—N angle of 175(1)°. The C—N bond lengths, for reasons of symmetry, are equal and refine to a value of 1.234(4) Å

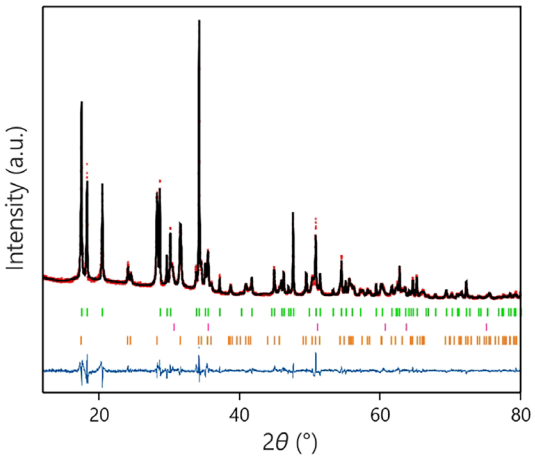

Figure 1. Rietveld fit of $Na_2Hf(NCN)_3$ to Cu-radiation PXRD data, showing observed (red), calculated (black), and difference (blue) intensities. Bragg positions of $Na_2Hf(NCN)_3$ (green), 4.49(1) wt% of HfO_2 $Fm\bar{3}m$ impurity (pink), and 29.2(4) wt% HfO_2 baddeleyite $P2_1/c$ impurity (orange) are denoted by vertical markers.

Table 1. Crystallographic data and fractional coordinates of $Na_2Hf(NCN)_3$.

Atom[a]	*x*	*y*	*z*	occ.	U_{iso}[10² Å²]
Na1	0	0	0.6679(1)	0.942(1)	2.01(9)
Hf2	"	"	"	1–occ.(Na1)	"
Hf1	0	0	0	0.883(2)	2.01(4)
Na2	"	"	"	1–occ.(Hf1)	"
N	0.9651(1)	0.6244(1)	0.2920(1)	1	1.72(5)
C	0.6344(1)	0	1/4	1	"

[a] $R\bar{3}c$, $Z = 6$, $a = 6.21134(5)$ Å, $c = 28.9629(4)$ Å; $R_{wp} = 7.10\%$, $R_p = 5.27\%$; $V = 967.70(2)$ Å³.

Table 2. Selected bond lengths and angles in $Na_2Hf(NCN)_3$.

Bond type	Bond length [Å]	Angle type	Bond angle [°]
Na—N	2.518(7), 2.497(8)	N—Na—N	170.2(2), 73.9(2), 100.4(2), 88.5(2), 97.7(2)
Hf—N	2.189(5)	N—Hf—N	92.98(5), 87.02(5)
C—N	1.234(4)	N—C—N	175(1)

supporting the presence of C=N double bonds. This can be well understood by considering the NCN coordination environment, where both ends of the carbodiimide anion coordinate similarly to one hafnium and two sodium atoms. The cation ordering motif between the layers, however, results in a slight tilt of 9.8(2)° and 5° bend of the NCN^{2-} anion away from the stacking axis in order to accommodate the size difference of $1.02 - 0.71 = 0.31$ Å between Na^+ and Hf^{4+} cations.[21] The NCN^{2-} shape is corroborated by the measured and phonon-based simulated IR spectrum given in **Figure 2**. We observe a splitting of the deformation vibration at 600 and 700 cm^{-1} and of the asymmetric vibration around 2100 cm^{-1}, thus affirming a bent $^-N{=}C{=}N^-$ carbodiimide as described in $MnHf(NCN)_3$.[22]

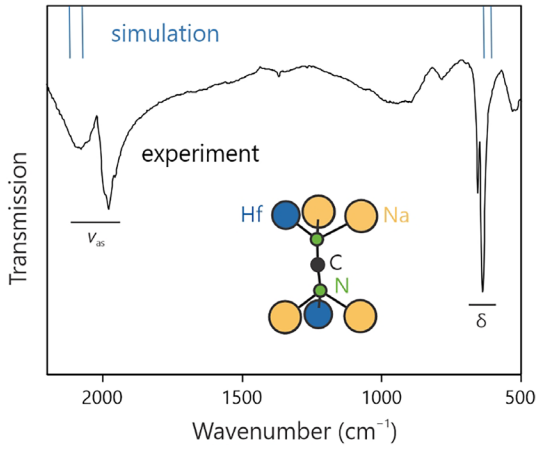

Figure 2. IR spectra of $Na_2Hf(NCN)_3$ (black, bottom) compared to the DFT-simulated (blue, top).

The site mixing present in $Na_2Hf(NCN)_3$ is comparable to that observed in the Li analog, where the similarity between the ionic radii of Li^+ and Hf^{4+} (0.76 Å and 0.71 Å for six-fold coordination, respectively) explains why the two cations may share sites.[19, 21] This criterion cannot be applied directly to $Na_2Hf(NCN)_3$, however, since in this case there is a considerable difference between the sizes of Na^+ (1.02 Å) and Hf^{4+} (0.71 Å), so explaining this site mixing requires a more in-depth analysis.[21]

$Na_2Hf(NCN)_3$ crystallizes in the same space group, $R\bar{3}c$, as the binary $M_2(NCN)_3$ compounds (M = Cr, Sc, Lu–Tm).[23–25] In $M_2(NCN)_3$, trivalent metal cations occupy two thirds of the available octahedral sites in a vacancy-ordered structure, where the M^{3+} ions are located at the 12*c* Wyckoff positions while the 6*b* sites remain vacant (**Figure 3**). By contrast, in $Na_2Hf(NCN)_3$, both sites are fully occupied, with the large Na^+ ions in the 12*c* position, so the relatively small Hf^{4+} ions occupy the 6*b* sites. Given that this structure type allows for vacancies, the analysis should focus on the effective surface area available for cationic accommodation rather than on the cationic size differential. Since the packing of NCN^{2-} anions determine the unit-cell volume, the area of the *ab* planes delimits the space for the metals in the layered structure. $Na_2Hf(NCN)_3$ has an available surface area per unit cell of $(a^2\sqrt{3})/2 \approx 33.4\text{Å}^2$, which is less than the maximum surface area reported for similar binary compounds $(a^2\sqrt{3})/2 \approx 34.8\text{Å}^2$ for $Tm_2(NCN)_3$.[25] This suggests that the site mixing obtained from the refinement is perfectly possible and consistent with the rest of the compounds in space group $R\bar{3}c$.

As previously mentioned, the ternary composition $Na_2T(NCN)_3$ can crystallize in two different space groups, $R\bar{3}c$ or *Pnna*, depending on whether *T* is Hf or Sn, respectively. To understand why $Na_2Hf(NCN)_3$ favors one structure over the other, density functional theory (DFT) calculations were performed to structurally optimize both the experimentally observed $R\bar{3}c$ structure and a hypothetical *Pnna* variant. The calculated values for the formation enthalpy at 0 K confirm the $R\bar{3}c$ as energetically favored over the *Pnna* structure by about 24 kJ mol^{-1} consistent with experiment.

A visual comparison of the two structural variants reveals different arrangements of the tetravalent cations in the two structures, leading to noticeably different Hf—Hf distances. In the $R\bar{3}c$ structure a triangular network arrangement with Hf—Hf distances of ≈5.97 Å is found while in the *Pnna* alternative a 1D channel arrangement with a shorter interchain Hf—Hf distance of 3.39 Å prevails (**Figure 4**), so more pronounced Hf−Hf interactions within *Pnna* are likely. This is corroborated by a simplified model of the pairwise Coulomb interactions, $E = (q_1 \times q_2)/r$, where q_1 and q_2 are the atomic Löwdin charges in question and *r* is the distance between them.[26–28] Applying this equation to $Na_2Hf(NCN)_3$ in the $R\bar{3}c$ structure results in a value for the repulsive interaction of $-(1.46 \times 1.46)/5.97e^2/\text{Å} = -0.35e^2/\text{Å}$. In the same way, a value of $-(1.47 \times 1.47)/3.39e^2/\text{Å} = -0.61e^2/\text{Å}$ is

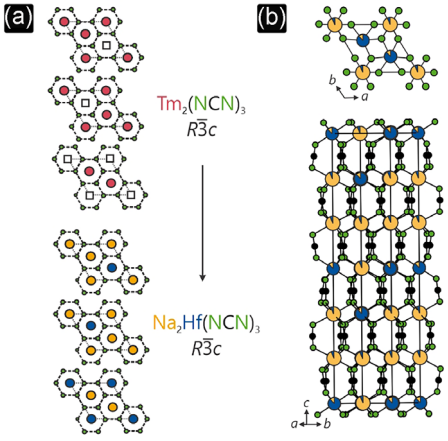

Figure 3. a) Schematic structural relation between $Tm_2(NCN)_3$ and $Na_2Hf(NCN)_3$ along the stacking direction. b) Crystal structure of $Na_2Hf(NCN)_3$.

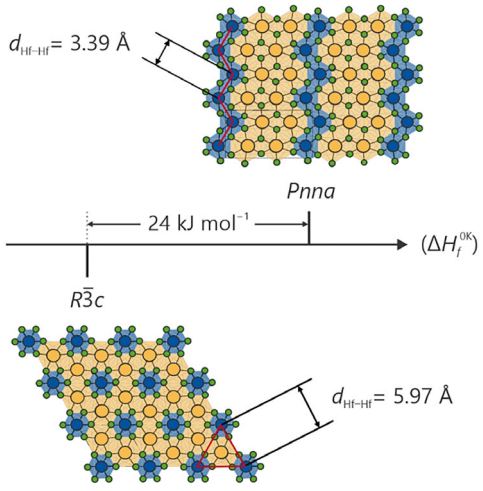

Figure 4. The formation enthalpy (ΔH) at 0 K of $Na_2Hf(NCN)_3$ in the *Pnna* structure compared to the most stable $R\bar{3}c$ configuration. HfN_6 octahedra are shown in blue, and NaN_6 octahedra in orange.

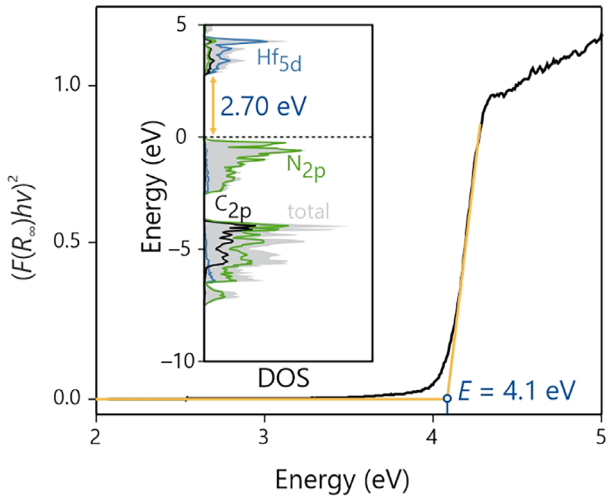

Figure 5. Tauc-plot of $Na_2Hf(NCN)_3$ for direct allowed transition and calculated total DOS (inset).

calculated for $Na_2Hf(NCN)_3$ in the *Pnna* structure, which clearly indicates about twice the repulsive interactions in the latter compound. We assume such repulsions to be responsible for the preference of $R\bar{3}c$ over *Pnna*.[29,30]

In turn, the electronic band structure of $Na_2Hf(NCN)_3$ was calculated for the fully relaxed $R\bar{3}c$ crystal structure. This yields a direct band gap of ≈2.7 eV. The valence and conduction band are dominated by the N 2p and Hf 5d levels, respectively. The optical bandgap was determined experimentally by UV–vis spectroscopy, giving a value of 4.1 eV coherent with a white sample, which is larger than the calculated data (**Figure 5**). This difference can be attributed to the generally recognized underestimation of the DFT-derived band gaps, in particular when using the PBEsol GGA-type functional.

3. Conclusions

Herein, we report the synthesis and characterization of $Na_2Hf(NCN)_3$, a ternary carbodiimide crystallizing in a NiAs-derived layered structure with $R\bar{3}c$ symmetry. In this phase, NCN^{2-} anions adopt a hexagonal close-packed arrangement, while cations fully occupy the octahedral interlayer sites. Rietveld refinements indicate a site disorder of ≈12%. Such disorder, as also reported in the lithium analog, can be explained by the space available for each of the cations in the $R\bar{3}c$ structure, which is more than sufficient to allow such disorder. The crystallization of $Na_2Hf(NCN)_3$ in the $R\bar{3}c$ space group is likely favored over *Pnna* due to stronger repulsive Hf—Hf interactions in the *Pnna* type since shorter Hf—Hf distances make it less energetically favorable. The experimental optical bandgap was measured at 4.1 eV, which is consistent with the white color of the sample and significantly higher than the calculated value of 2.7 eV. Such a difference was attributed to the recognized underestimation of the band gaps by DFT. Future research will focus on investigating sodium ionic conductivity for potential application in sodium-ion batteries.

4. Experimental Section

Synthesis: Na_2NCN was prepared as described in ref. [29] and further dried at 200 °C under dynamic vacuum. Before use, $HfCl_4$ (Thermo Fisher 98%) was further purified by sublimation at 180 °C under dynamic vacuum. Na_2NCN and $HfCl_4$ were mixed in a 3:1 molar ratio in an agate mortar and sealed into an evacuated ($p = 10^{-3}$ mbar) quartz ampoule. The reaction mixtures were then heated up to 700 °C, remaining at this temperature for 10 h with a heating and cooling rate of 2 °C min^{-1}. Longer annealing time did not result in better crystallinity. The reaction equation is given below.

$$3Na_2NCN + HfCl_4 \rightarrow Na_2Hf(NCN)_3 + 4NaCl \quad (3)$$

The white colored reaction product, $Na_2Hf(NCN)_3$, proved to be air and water stable. Therefore, the coproduced metathesis salt NaCl was removed by washing with water. Alongside the formation of the ternary $Na_2Hf(NCN)_3$ phase, HfO_2 was also identified, which is likely attributable to the pronounced moisture sensitivity of the $HfCl_4$ precursor.

PXRD Analysis: PXRD measurement on $Na_2Hf(NCN)_3$ was carried out at room temperature using a calibrated STOE STADI-P powder diffractometer with flat sample holders (Cu $K_{\alpha 1}$, linear PSD, 2θ range 2-65° with individual steps of 0.005°). Rietveld refinements were performed using GSAS with the EXPGUI interface.[30] The thermal displacement parameters U_{iso} of the light atoms C and N were constrained to be equal. Similarly, those of metal cations occupying the same site were constrained to be equal. Furthermore, structural refinements reveal a conspicuous partial disorder between Hf and Na on opposite sites. A partial disorder of the order of around 12(1)% was concluded, with clear improvements in fits dropping from a value of $R_{wp} = 9.23\%$ without site mixing to a value of $R_{wp} = 7.10\%$ with site mixing. Full details concerning the structure determination including all intensity data are available in CIF format and have been deposited under the CCDC entry number 2480148.

Infrared Measurements: Infrared spectroscopy measurement was recorded on a Shimadzu IRSpirit FT-IR spectrometer.

UV−Vis Measurements: UV−Vis spectra were recorded on a Shimadzu UV-2006 spectrophotometer. A Tauc plot was calculated via the Kubelka−Munk function $F(R) = (1-R)^2/2R$ to determine the bandgap size.

Computational Details: To understand the structural preference of $Na_2Hf(NCN)_3$, the enthalpies of formation were calculated for *Pnna* and R_{3c} modifications. The following theoretical reaction equation starting from the elements was used to calculate $\Delta H_{formation}$ based on DFT.

$$\Delta H_{formation} = E(Na_2Hf(NCN)_3) - 2 \times E(Na) - E(Hf) - 3 \times E(N_2) - 3 \times E(C) \quad (4)$$

All entries for this reaction equation as well as both $Na_2Hf(NCN)_3$ modifications were optimized using Blöchl's Projector Augmented Wave (PAW)[31] method as implemented in the Vienna ab initio simulation package (VASP) v.6.4.1.[32–35] Electronic exchange and correlation were described using the functional of Perdew, Burke, and Ernzerhof optimized for solids (PBEsol).[36,37] The convergence criteria were set to energetic differences of $\mathbf{10^{-8}}$ eV for electronic and $\mathbf{10^{-6}}$ eV for ionic optimizations. The energy cutoff of the plane-wave basis set was set to 700 eV. The Monkhorst–Pack scheme[38] was used to generate *k*-point meshes, yielding $\mathbf{9 \times 9 \times 3}$ and $\mathbf{11 \times 7 \times 7}$ for the $\boldsymbol{R\bar{3}c}$ and *Pnna* structure respectively. Brillouin-zone integrations were carried out using Blöchl's tetrahedron method.[39] The wave functions of the optimized structures were projected onto an atomic-orbital

basis using LOBSTER v.5.1.1 (Local orbital basis suite towards electronic-structure reconstruction).[40–45] This way, Density of States (DOS), Crystal–Orbital Bond Indices (COBI), and their energy integrals (ICOBI) as well as Löwdin charges were automatically determined from LOBSTER. The atomic-orbital basis set pbeVASPfit2015[43] was used. Phonon calculations were carried out for $4 \times 4 \times 1$ ($R\bar{3}c$) and $3 \times 2 \times 2$ (*Pnna*) supercells of the fully relaxed structures using phonopy v.2.7.17[46] The phonon calculations served as a basis for the simulation of the IR spectrum using the IRprogram package v.1.0.2.[47–50]

Acknowledgements

We thank Tobias Storp for his assistance with PXRD measurements. Juan Medina-Jurado is grateful for the financial support from Deutscher Akademischer Austauschdienst (DAAD).

Open Access funding enabled and organized by Projekt DEAL.

Conflict of Interest

The authors declare no conflict of interest.

Data Availability Statement

The data that support the findings of this study are openly available in [CCDC] at [https://www.ccdc.cam.ac.uk/], reference number [2480148].

Keywords: carbodiimides · characterization · density functional theory · synthesis · X-ray diffraction

[1] H.-J. Meyer, *Dalton Trans.* **2010**, *39*, 5973.
[2] M. G. Down, M. J. Haley, P. Hubberstey, R. J. Pulham, A. E. Thunder, *Dalton Trans.* **1978**, *10*, 1407.
[3] M. Becker, J. Nuss, M. Jansen, *Z. Anorg. Allg. Chem.* **2000**, *626*, 2505.
[4] M. Becker, M. Jansen, *Acta Crystallogr., Sect. C: Struct. Chem.* **2001**, *57*, 347.
[5] X. Reckeweg, F. J. DiSalvo, *Z. Anorg. Allg. Chem.* **2003**, *629*, 177.
[6] N.-G. Vannerberg, G. Claeson, L. Schotte, A. Block-Bolten, J. Toguri, H. Flood, *Acta Chem. Scand.* **1962**, *16*, 2263.
[7] U. Berger, W. Schnick, *J. Alloys Compd.* **1994**, *206*, 179.
[8] X. Liu, M. Krott, P. Müller, C. Hu, H. Lueken, R. Dronskowski, *Inorg. Chem.* **2005**, *44*, 3001.
[9] G. Baldinozzi, B. Malinowska, M. Rakib, G. Durand, *J. Mater. Chem.* **2002**, *12*, 268.
[10] X. Liu, L. Stork, M. Speldrich, H. Lueken, R. Dronskowski, *Chem. - Eur. J.* **2009**, *15*, 1558.
[11] M. Krott, X. Liu, B. P. T. Fokwa, M. Speldrich, H. Lueken, R. Dronskowski, *Inorg. Chem.* **2007**, *46*, 2204.
[12] R. Pöttgen, A. J. Corkett, R. Dronskowski, *Z. Kristallogr.* **2023**, *238*, 95.
[13] M. Kubus, R. Heinicke, M. Ströbele, D. Enseling, T. Jüstel, H.-J. Meyer, *Mater. Res. Bull.* **2015**, *62*, 37.
[14] J. Medina-Jurado, F. Grysla, H. Bourakhouadar, D. Chen, A. J. Corkett, R. Dronskowski, *J. Solid State Chem.* **2024**, *340*, 0022.
[15] L. Unverfehrt, M. Ströbele, H.-J. Meyer, *Z. Anorg. Allg. Chem.* **2013**, *639*, 22.
[16] A. J. Corkett, K. Chen, R. Dronskowski, *Eur. J. Inorg. Chem.* **2020**, *2020*, 2596.
[17] A. J. Corkett, M. Okhrymenko, V. Roddatis, O. I. Lebedev, J. Van Leusen, R. E. G. Delina, J. P. H. Perez, L. G. Benning, R. Dronskowski, *Inorg. Chem.* **2025**, *64*, 2886.
[18] L. Unverfehrt, M. Ströbele, J. Glaser, H.-J. Meyer, *Z. Anorg. Allg. Chem.* **2009**, *635*, 1947.
[19] K. Dolabdjian, C. Castro, H.-J. Meyer, *Eur. J. Inorg. Chem.* **2018**, *44*, 1624.
[20] H. Bourakhouadar, J. Medina-Jurado, P.-C. Müller, A.-J. Corkett, R. Dronskowski, *Dalton Trans.* **2024**, *53*, 19272.
[21] R. Shannon, *Acta Crystallogr., Sect. A* **1976**, *32*, 751.
[22] H. Bourakhouadar, J. Hempelmann, J. van Leusen, A. Drichel, L. Bayarjargal, A. Koldemir, M. K. Reimann, R. Pöttgen, A. Slabon, A. J. Corkett, R. Dronskowski, *J. Am. Chem. Soc.* **2024**, *146*, 26071.
[23] X. Tang, H. Xiang, X. Liu, M. Speldrich, R. Dronskowski, *Angew. Chem., Int. Ed.* **2010**, *49*, 4738.
[24] P. Kallenbach, M. Ströbele, H.-J. Meyer, Z. Anorg. *Allg. Chem.* **2020**, *646*, 1281.
[25] M. Neukirch, S. Tragl, H.-J. Meyer, *Inorg. Chem.* **2006**, *45*, 20.
[26] M. Coulomb, *Hist. Acad. Roy. Sci.* **1785**, 569.
[27] M. Coulomb, *Hist. Acad. Roy. Sci.* **1785**, 578.
[28] M. Coulomb, *Hist. Acad. Roy. Sci. 1785*, 612.
[29] A. O. Corral, M. Kubus, M. Ströbele, H.-J. Meyer, *Z. Anorg. Allg. Chem.* **2014**, *640*, 902.
[30] B. H. Toby, *J. Appl. Crystallogr.* **2001**, *34*, 210.
[31] P. E. Blöchl, *Phys. Rev. B* **1994**, *50*, 17953.
[32] G. Kresse, J. Hafner, *Phys. Rev. B* **1993**, *47*, 558.
[33] G. Kresse, J. Furthmüller, *Comput. Mater. Sci.* **1996**, *6*, 15.
[34] G. Kresse, J. Furthmüller, *Phys. Rev. B* **1996**, *54*, 11169.
[35] G. Kresse, D. Joubert, *Phys. Rev. B* **1999**, *59*, 1758.
[36] J. P. Perdew, *Int. J. Quantum Chem.* **2009**, *28*, 497.
[37] J. P. Perdew, A. Ruzsinszky, G. I. Csonka, O. A. Vydrov, G. E. Scuseria, L. A. Constantin, X. Zhou, K. Burke, *Phys. Rev. Lett.* **2009**, *102*, 136406.
[38] H. J. Monkhorst, J. D. Pack, *Phys. Rev. B* **1976**, *13*, 518.
[39] P. E. Blöchl, O. Jepsen, O. K. Andersen, *Phys. Rev. B* **1994**, *49*, 16223.
[40] R. Dronskowski, P. E. Blöchl, *J. Phys. Chem.* **1993**, *97*, 8617.
[41] V. L. Deringer, A. L. Tchougréeff, R. Dronskowski, *J. Phys. Chem. A* **2011**, *115*, 5461.
[42] S. Maintz, V. L. Deringer, A. L. Tchougréeff, R. Dronskowski, *J. Comput. Chem.* **2013**, *34*, 2557.
[43] S. Maintz, V. L. Deringer, A. L. Tchougréeff, R. Dronskowski, *J. Comput. Chem.* **2016**, *37*, 1030.
[44] R. Nelson, C. Ertural, J. George, V. L. Deringer, G. Hautier, R. Dronskowski, *J. Comput. Chem.* **2020**, *41*, 1931.
[45] P. C. Müller, C. Ertural, J. Hempelmann, R. Dronskowski, *J. Phys. Chem. C* **2021**, *125*, 7959.
[46] A. Togo, I. Tanaka, *Scr. Mater.* **2015**, *108*, 1.
[47] J. George, R. Dronskowski, IR Version 1.0.2, Zenodo, **2018**, https://doi.org/10.5281/zenodo.1168026.
[48] D. Karhánek, T. Bučko, J. Hafner, *J. Phys.: Condens. Matter* **2010**, *22*, 265006.
[49] P. Giannozzi, S. Baroni, *J. Chem. Phys.* **1994**, *100*, 8537.
[50] A. Görne, J. George, J. van Leusen, R. Dronskowski, *Inorganics* **2017**, *5*, 10.

Manuscript received: August 15, 2025
Revised manuscript received: September 7, 2025
Version of record online: September 22, 2025

